Early Results from the *XMM-Newton* EPIC Calibration Observations of the Young Open Cluster NGC 2516

S. Sciortino[1], G. Micela[1], F. Damiani[1], E. Flaccomio[1], K. Briggs[2], M. Demby[2], J. Pye[2], N. Grosso[3], A. M. Read[3], P. Gondoin[4], and R. D. Jeffries[5]

[1]Osservatorio Astronomico di Palermo G.S. Vaiana, Piazza del Parlamento 1, 90134 Palermo, Italy
[2]X-ray Astronomy Group, Department of Physics & Astronomy, University of Leicester, Leicester, LE1 7RH, UK
[3]Max-Planck-Institut für Extraterrestrische Physik, Postfach 1312, 85741 Garching, Germany
[4] European Space Research and Technology Center, 2200 AG Noordwijk ZH, The Netherlands
[5]Department of Physics and Astronomy, Keele University, Staffordshire, ST5 5GB, UK

Abstract. We present early results of the analysis of *XMM-Newton* calibration data of the young open cluster NGC 2516. In a 20 ks EPIC observation taken with the thick filters, we have found 109 X-ray sources that have been simultaneously detected in the two EPIC MOS Cameras. We have reached a limiting sensitivity of $\sim 10^{-3}$ cnt/sec in the 0.3-8.0 keV bandpass (i.e. $\sim 7\ 10^{-15}$ erg sec^{-1} cm^{-2}). A sizeable fraction of EPIC sources have also been observed and detected in the NGC 2516 *Chandra* PV observations. For the sources in common we have found that the XMM/EPIC and Chandra/ACIS-I fluxes compare well. Preliminary identifications based on a 1 sq. deg. CCD survey extending down to V $\sim$ 20 confirm that a large fraction of sources are associated with likely cluster members.

1. Why NGC 2516 ?

NGC 2516 has been chosen as an calibration target of the *XMM-Newton* observatory (Jansen et al. 2001) in order to "bore sight" the alignment of the X-Ray telescope as well as the relative positions of the EPIC cameras CCDs since it is a rich region of X-ray emitting young stars.

2. Why NGC 2516 is a Crucial Stellar Target ?

Apart from this role in the early phase of *XMM-Newton* mission, NGC 2516 plays an important role in the study of stellar physics. NGC 2516 is a southern, relatively nearby ($\sim$ 387 pc), open cluster with metallicity below solar ([Fe/H] = -0.32) and an age ($\sim 10^8$ yr) similar to that of the Pleiades.

Because of its metallicity, it plays a crucial role in exploring the relation between stellar structure, metallicity, and coronal emission level. Such a relation is expected to exist since the metallicity affects the depth of the convection zone that in turn should affect the efficiency of dynamo action of which X-ray luminosity is a proxy (see also discussion in Micela et al. 2000). Indeed Jeffries et al. (1997), based on ROSAT PSPC data, have found that the most X-ray luminous dG NGC 2516 members are less luminous than the most X-ray luminous solar-metallicity, similar age, dG in the Pleiades. The avalaibility of deeper and higher spatial resolution *XMM-Newton* (as well as *Chandra*) data allow us to investigate this matter on more solid grounds.

3. *XMM-Newton* NGC 2516 Calibration Data

At the end of the calibration phase NGC 2516 has been observed 4 times, as indicated in the table below. The four data sets are not of the same quality, not only because of their different exposure times, but also because of the occurrence of rapid increases in the background level that occurs during part of the first, third and fourth observations.

Table 1. Summary of NGC 2516 *XMM-Newton* Calibration Data until July 1-st 2000

Obs ID	RA_{J2000} (h m s)	Dec_{J2000} (d m s)	Exp. Time[a] (ksec)	Clean Exp.Time[b] (ksec)	Obs Date
1	7 58 33	-60 52 54	7.7	7.2	12 March 2000
2	7 58 29	-60 53 32	20.0	18.6	6 April 2000
3	7 58 29	-60 53 32	17.0	15.1	7 April 2000
4	7 58 18	-60 47 13	29.2	22.8	10 June 2000

a - Exposure times are for the PN camera. The MOS camera ones usually differ only by a few hundreds of seconds, except for observation 4 for which MOS exposure times are $\sim$ 2 ks shorter. b - Cleaned exposure times are essentially the same for MOS and PN cameras.

4. Examples of Available Data

Figures 1 and 2 show the data of the MOS1 and MOS2 Cameras (Turner et al. 2001) for the second observation. Each dot in the image represents one of the collected X-ray photons in the 0.3-8.0 keV range, dots have been color coded according to photon energy, as indicated by the color scale at the bottom of figures. The 15” radius circles are centered at the source positions in MOS1 and MOS2 cameras, respectively.

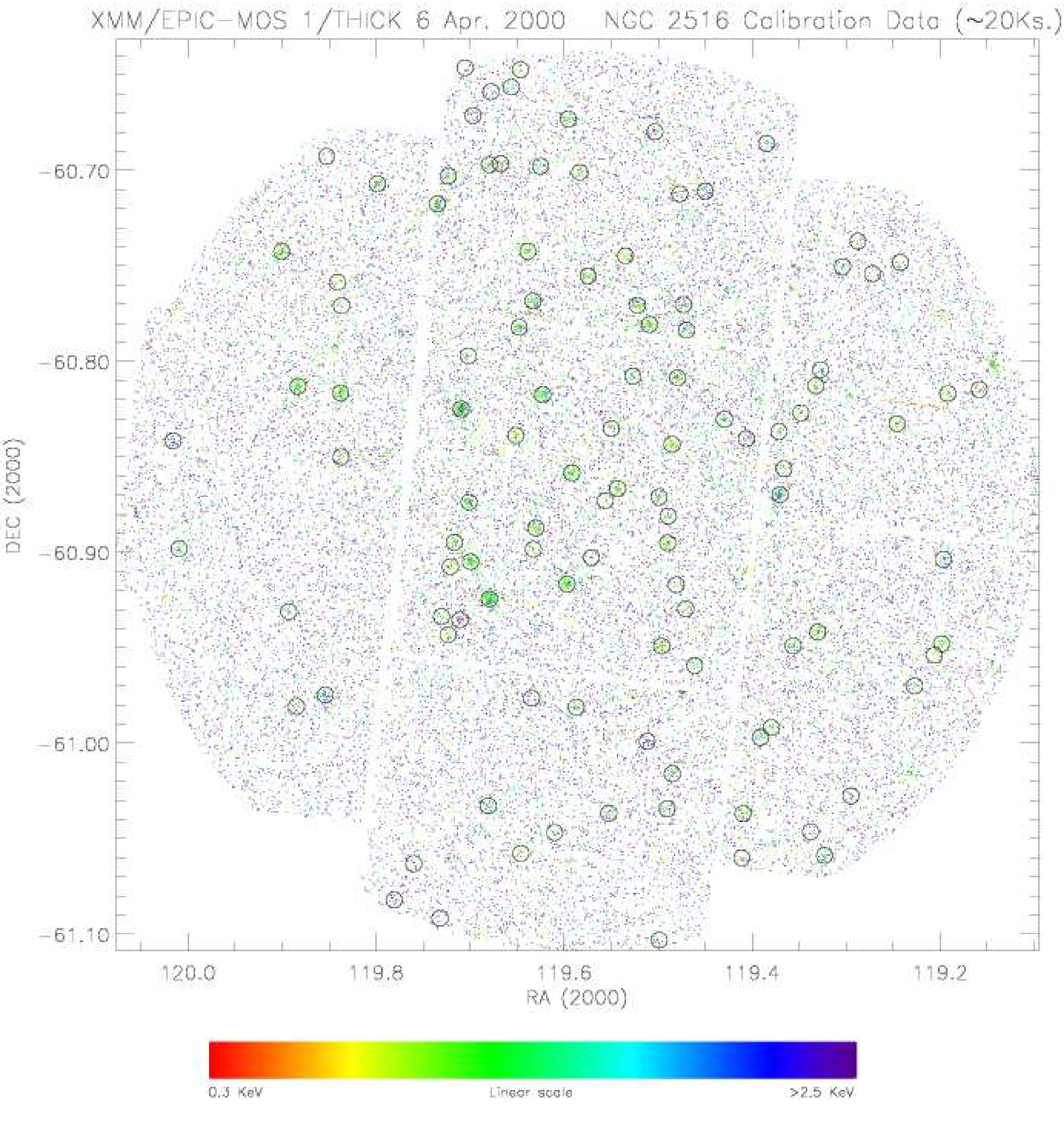

Figure 1 - EPIC MOS1 data for the 2-nd observation.

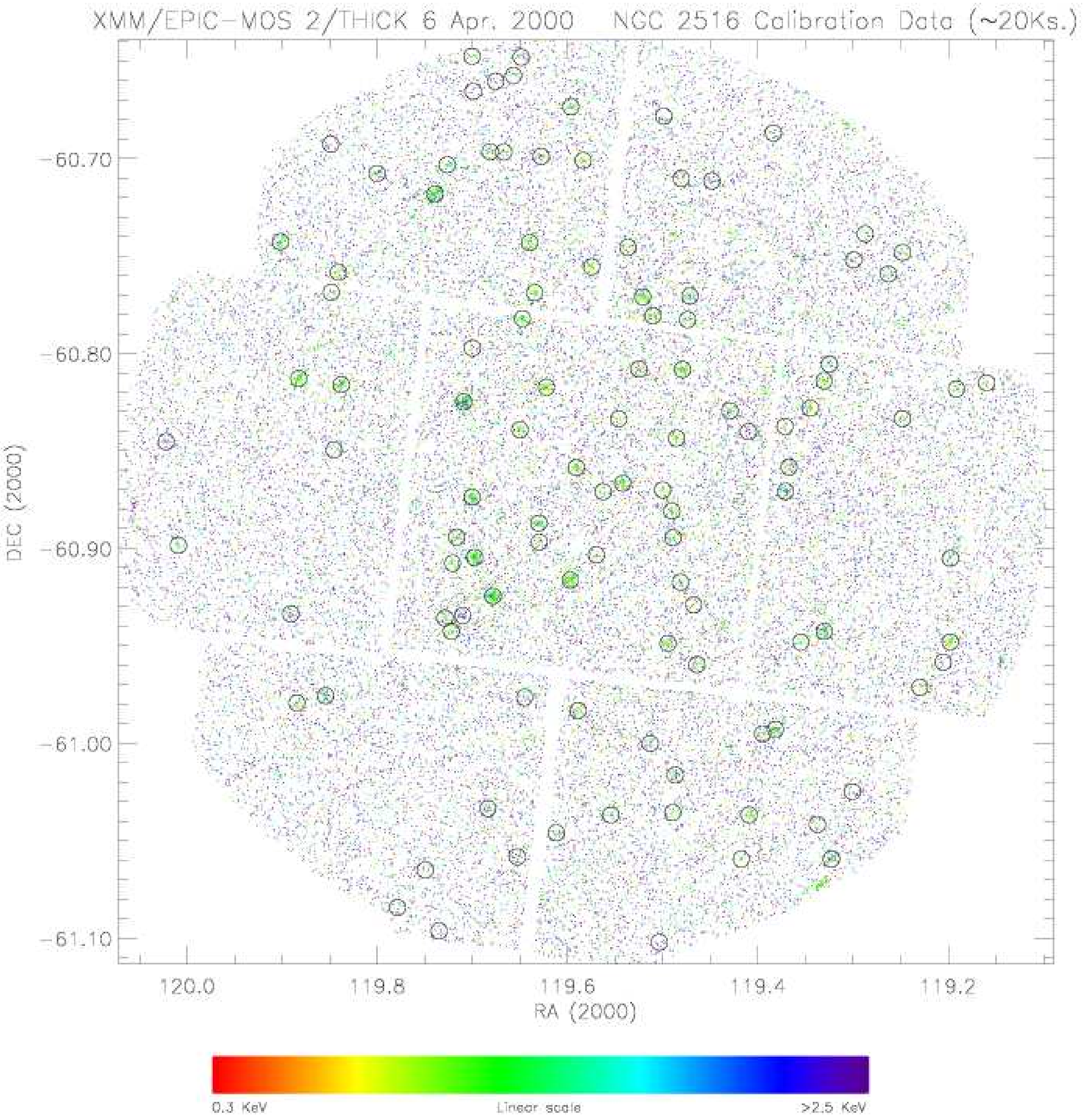

Figure 2 - EPIC MOS2 data for the 2-nd observation.

Fig. 3 shows the data of the PN camera (Strüder et al. 2001) for the same observation. Photons are color coded according to their energy as in Figs. 1 and 2.

5. Improving Quality of Available Data

Given the occurrence of strong and rapid variation in the background level associated with the external spacecraft environment, in order to detect sources as weak as possible it is important to time filter the data. We have developed a simple, but effective criterion based on the optimization of the source S/N ratio, that operating on a binned light curve of image-rate[1] is able to identify the offending time intervals. Its operation is illustrated in Fig. 4 that shows, in two cases, the image-rate as a function of time. All bins (i.e. time intervals) above the red-line have to be rejected since their inclusion will result in a reduction, in the background limited regime, of the attainable source S/N. Note that this effect is virtually absent in the second observations we have analyzed in the present paper.

The relevance of time-filtering is shown in Figs. 5 and 6, where we compare, using the same false-color scale within each pair, intensity images before and after the application of our time filtering technique. This is an important step in order to extend the analysis to all other available datasets and be able to reach the deepest limiting sensitivity in order to detect the low-mass cluster members.

6. Detections, Source Properties and Limiting Sensitivity

In this paper we present the analysis of the MOS1 and MOS2 data of the second observation. A more extensive analysis including also the third observation and a detailed account of scientific results is given by Sciortino et al. (2001). Some of these results are reviewed by Micela (2001). The analysis presented here has made use of standard SAS V4.1 tools, plus some additional tools written in IDL. Data have been processed with the standard *emchain* and *epchain*, and have been screened, rejecting non-X-ray events on the basis of their characteristics (like pattern, quality flag, etc.). In the case of PN data we have screened out one additional "hot" column from CCD chip number 5. Sources have been searched separately in MOS1 and MOS2 cameras using the standard SAS V4.1 *edetecproc* tool in 4 distinct energy bands, namely: 0.3-0.8 keV, 0.8-2.4 keV, 2.4-4.0 keV, 4.0-8.0 keV. As a starting point we have adopted a very low maximum-likelihood source acceptance threshold (ML=7), and then we have retained only the sources detected in both cameras and matched positionally within an angular separation of 25". With this procedure we have a (conservative) list of 109 distinct sources.

Figures 7 and 8 summarize some of the source properties as seen with the MOS1 and MOS2 cameras. For the weakest source we have collected ~ 15 counts (in each camera), while for the strongest source we have collected about 334 counts. In deriving X-ray flux we have assumed a conversion factor from counts to flux in the 0.3-8.0 keV bandpass of 7.1 10^{-12} erg cm^{-2}/count, computed with PIMMS for a Raymond-Smith spectrum with kT=0.54 keV and $N_H = 7.5\ 10^{20}$ cm^{-2}. Hence, with a single MOS image, we have reached the limiting sensitivity ($\sim 7\ 10^{-15}$ erg sec cm^{-2}), achieved by the 60 ks ROSAT PSPC observation analyzed by Jeffries et al. (1997), but with a better spatial resolution. Deeper

[1]For the current observations the image rate is largely dominated by background counts.

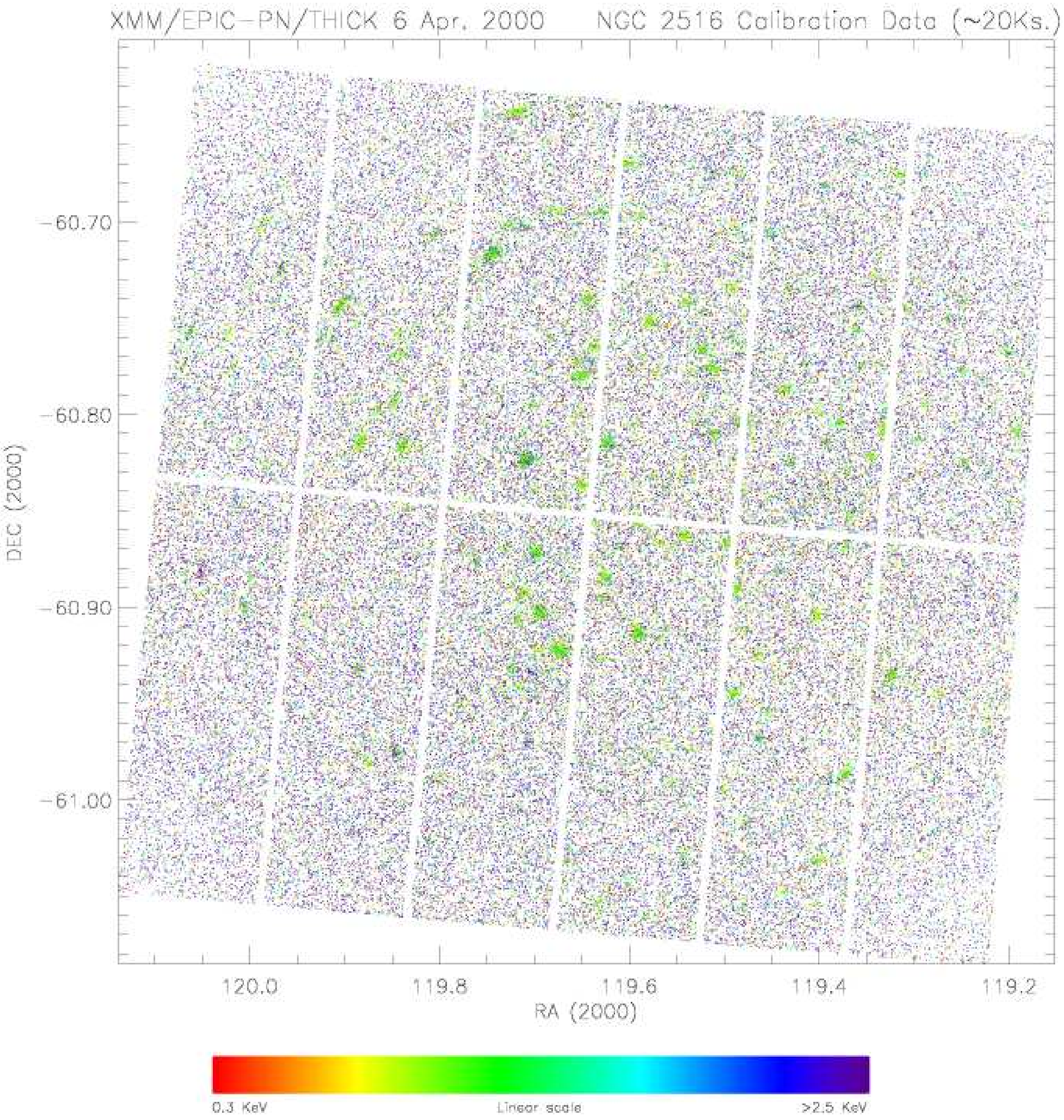

Figure 3 - EPIC PN data for the 2-nd observation.

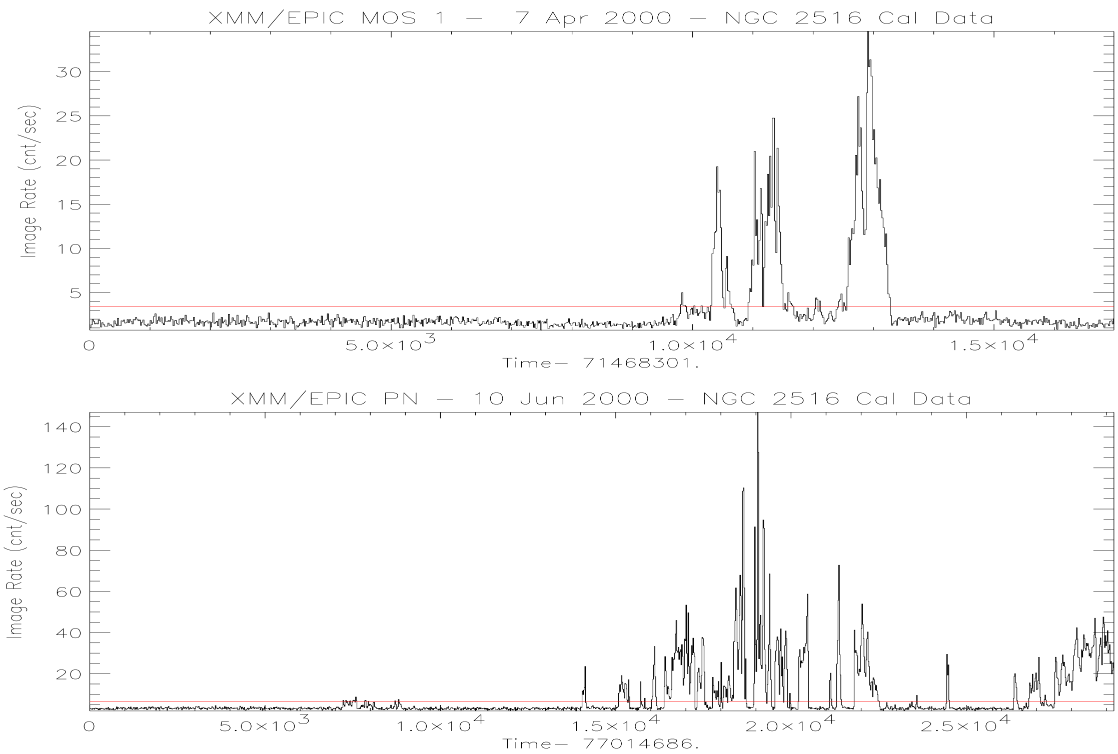

Figure 4 - Image rates as a function of time for two distinct observations and for two distinct cameras. The red horizontal lines mark the level of maximum admissible image rate above which the limiting sensitivity decrease (instead of increasing) with the further addition of exposure time. All bins in which the image rate is above the value indicated by the red line have to be rejected in order to detect faint sources and made an optimal use of available data.

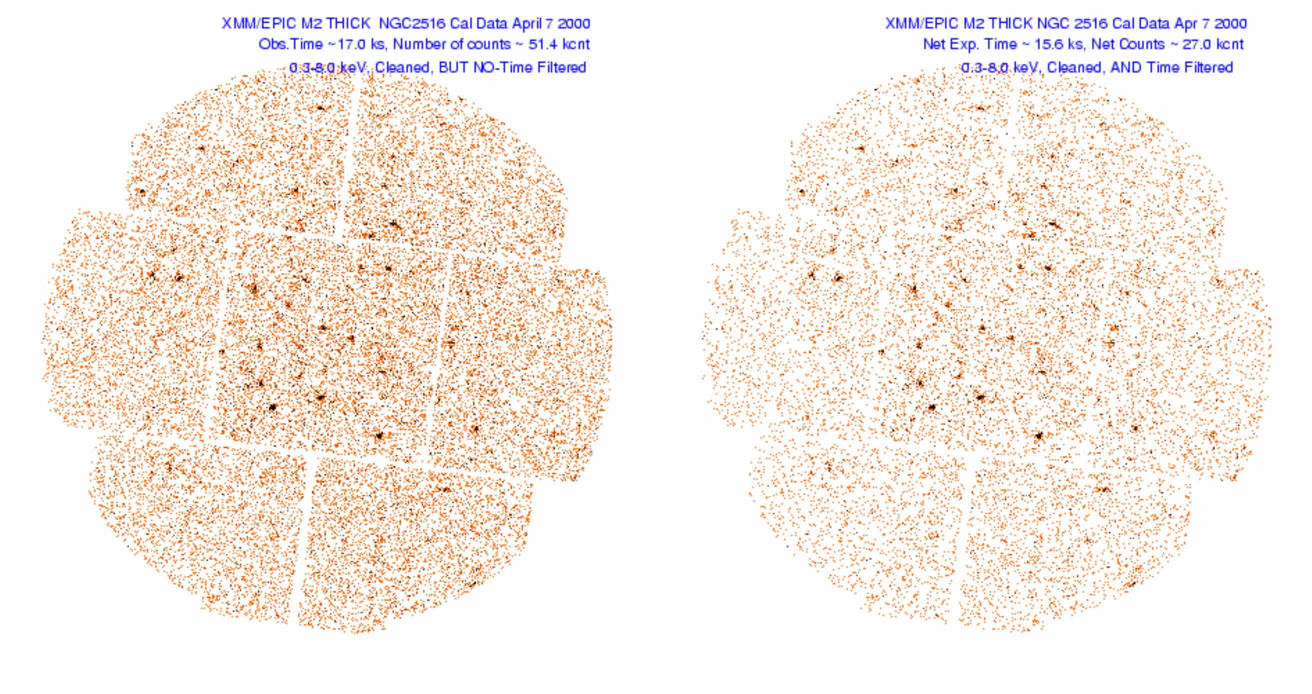

Figure 5 - Comparison of time-filtering effect on the data collected with the MOS2 camera during the 3-rd observation. Left, unfiltered; Right, filtered

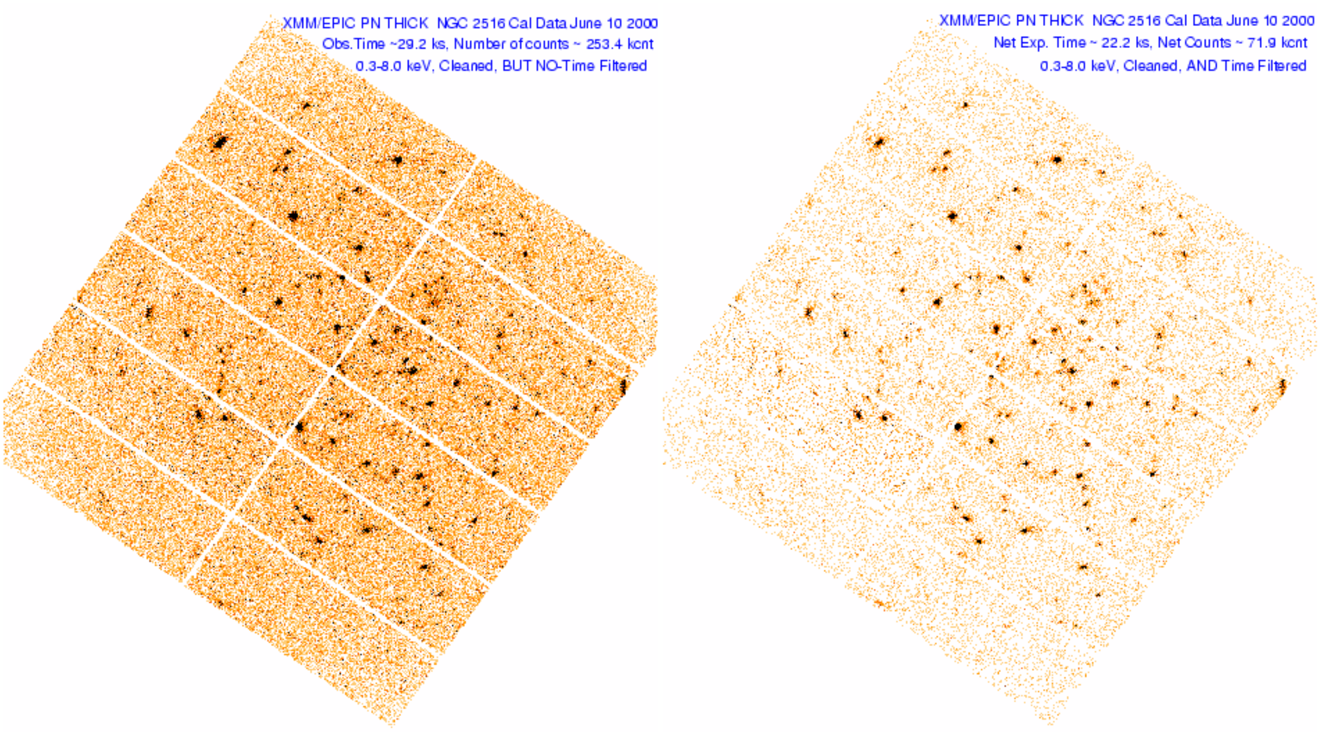

Figure 6 - Comparison of time-filtering effect on the data collected with the PN camera during the 4-th observation. Left, unfiltered; Right, filtered

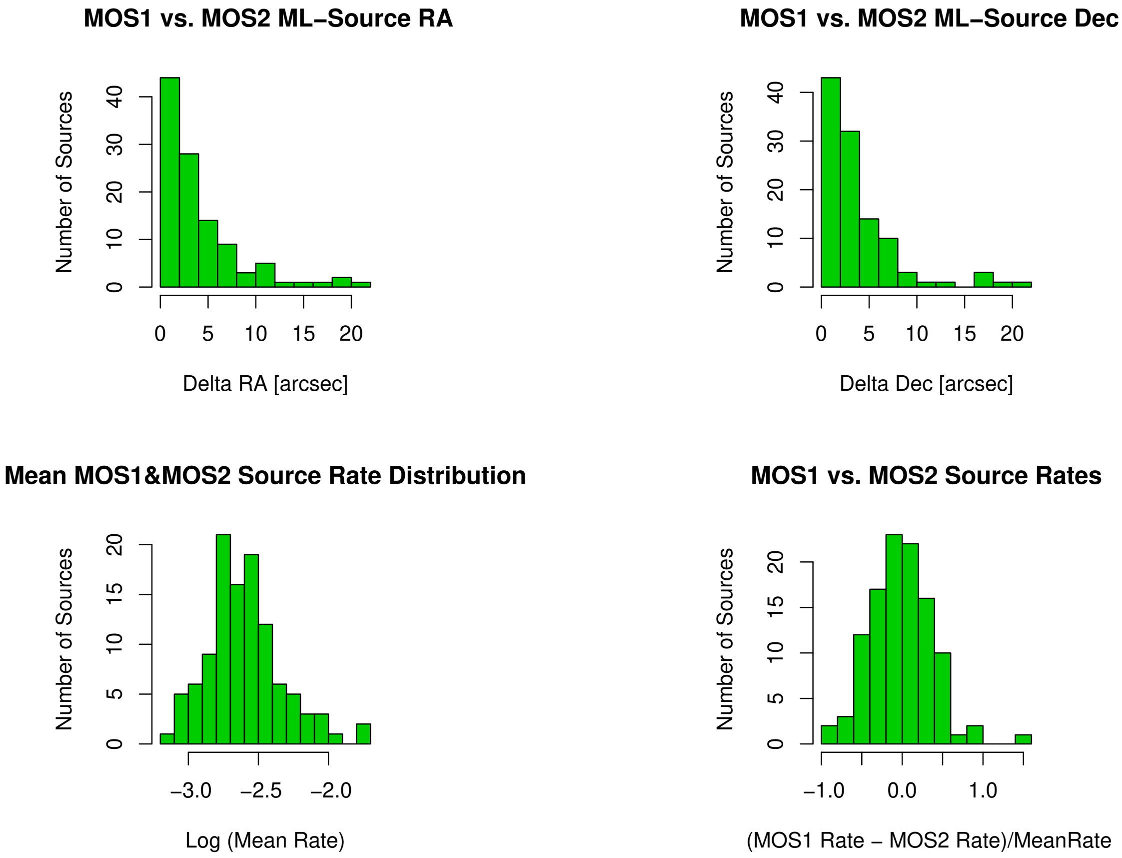

Figure 7 - For the majority of sources MOS1 and MOS2 rates differ no more than 40%.

sensitivity can be reached combining all available observations and combining data from the three cameras (cf. Sciortino et al. 2001).

7. Current Positional Accuracy

The overall attained positional accuracy is quite good and is within expectations. This is clearly shown in Fig. 9, where we have overlayed on the DSS image circles of 15” radius centered at source positions (defined as mean values derived from the analysis of MOS1 and MOS2 data). The astrometrc system of MOS cameras is currently better than few arcseconds.

8. Comparison with *Chandra* PV data

We have positionally matched the list of 147 sources found by Harnden et al. (2000) analyzing a 20ks ACIS-I *Chandra* observation with the sources we have found in MOS1 and MOS2 cameras. Assuming a cross-matching separation of 15” we have found 70 and 60 matches with MOS1 and MOS2 sources, respectively. In Fig. 10 we show a comparison among the ACIS and the MOS1 and MOS2 rates and fluxes.

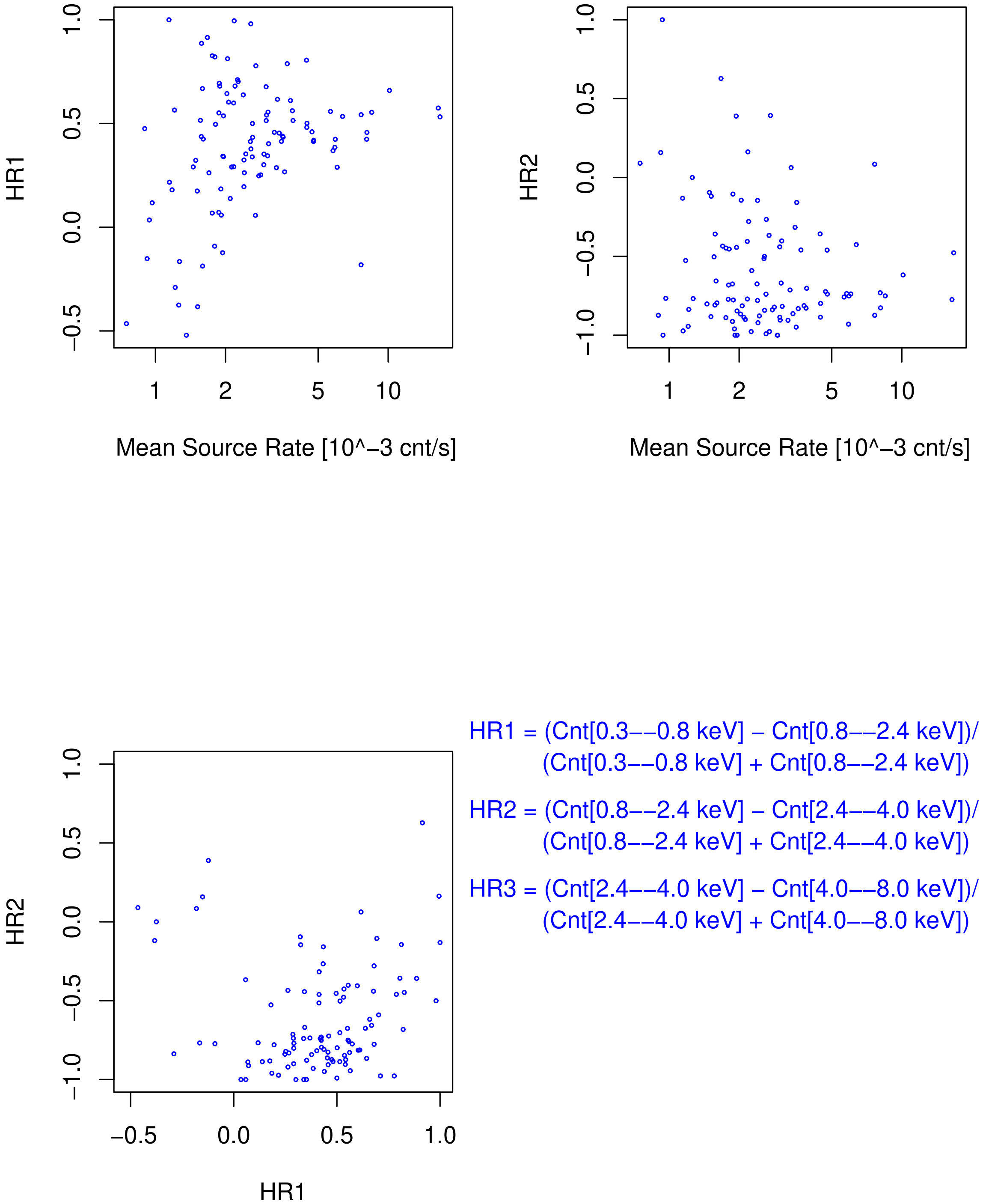

Figure 8 - Note the six sources that occupy a distinctly different region of the HR1-HR2 plane with respect to the majority of sources.

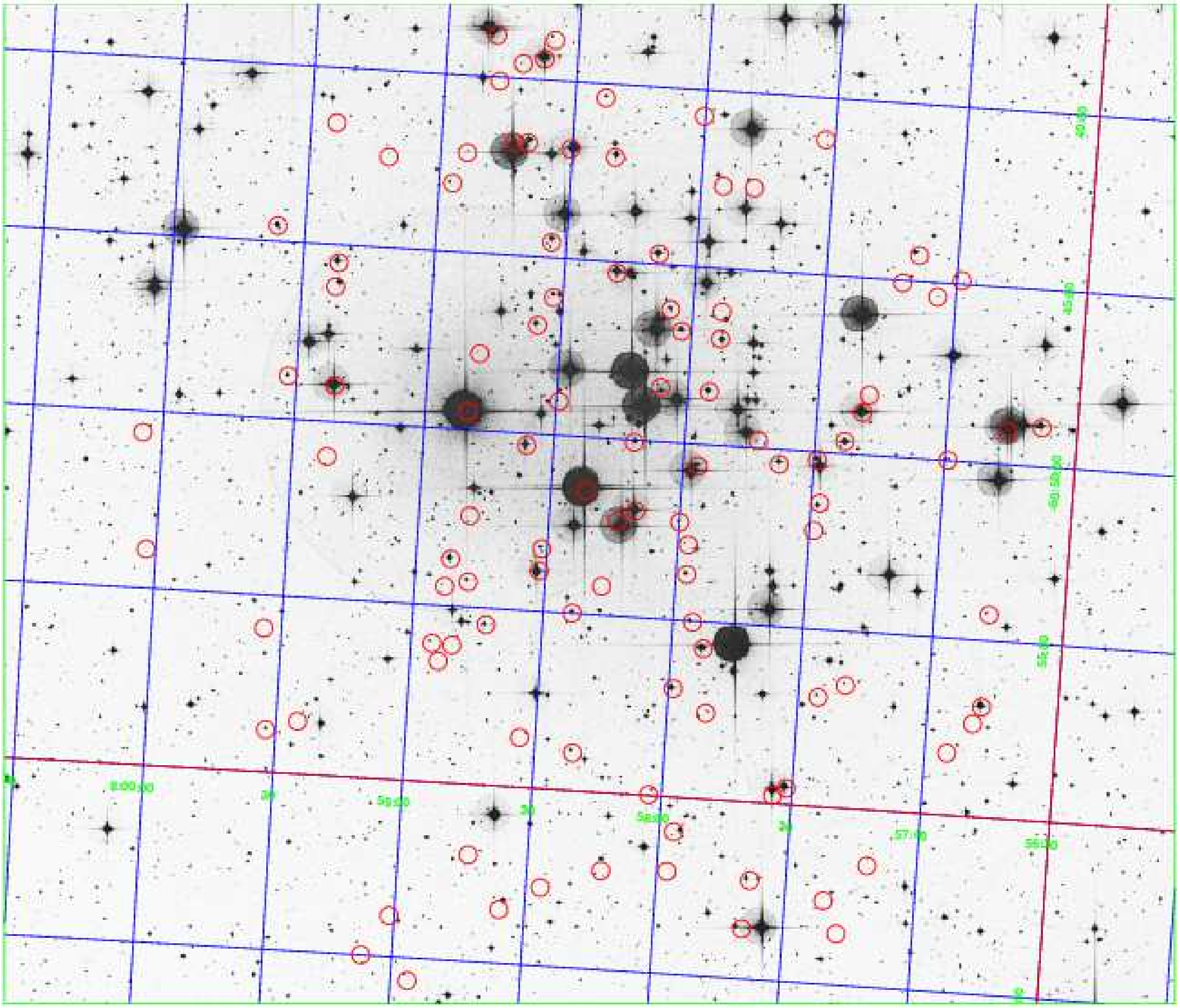

Figure 9 - Optical image of the central part of the NGC 2516 region surveyed with *XMM-Newton.* The red circle of 15" of radius are centered at the positions of the X-ray sources. Note the agreement between optical and X-ray positions.

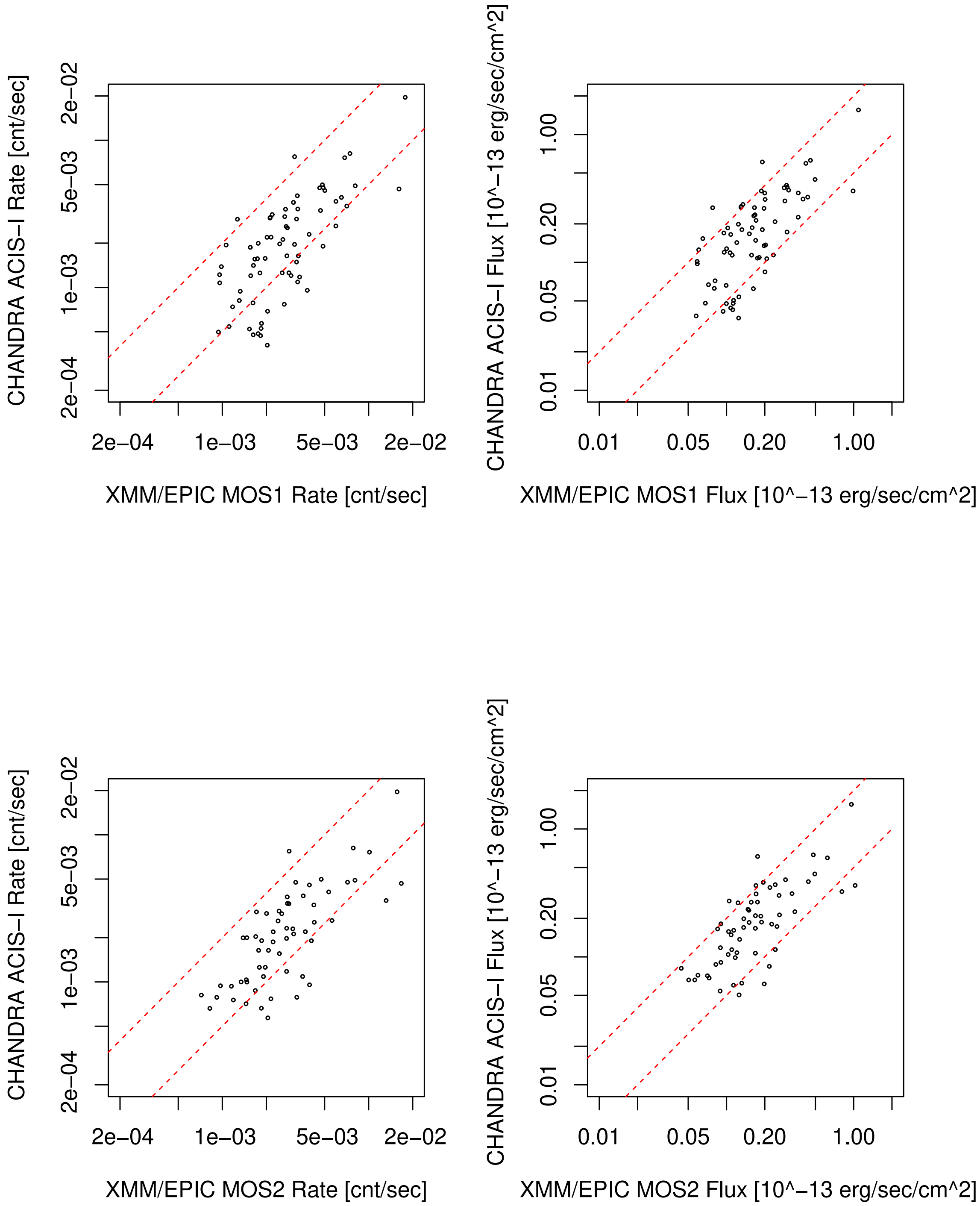

Figure 10 - Note that the *XMM-Newton* and the *Chandra* derived fluxes match within a factor 2 (as outlined by the dashed lines).

9. Optical Identifications

We have identified the MOS1 and MOS2 sources detected with Maximum Likelihood greater than 10 with the optical catalogue derived from a 1 sq. deg. CCD survey (Jeffries, Thurston and Hambley, in preparation). We have assumed a matching radius of 6". In Fig. 11 we show the CMDs for the sub-sample of objects within the field of view of the MOS1/MOS2 cameras (black dots), while the identified objects are marked with red symbols. We note that in the above field of view fall $\sim$ 430 photometric cluster members out of a total of $\sim$ 3300 objects.

10. Short-Term Variability

We have started to investigate the short-term variability of X-ray sources. In Fig. 12 we show a nice example of a flare seen on the early F DK92 star. This is one of the few example of intence flare seen on a early dF star.

Acknowledgments. Based on observations obtained with *XMM-Newton*, an ESA science mission with instruments and contributions directly funded by ESA Member States and the USA (NASA). EPIC was developed by the EPIC Consortium (P.I., Dr. M. J. L. Turner). The consortium comprises the following Institutes: University of Leicester, University of Birmingham, (UK); CEA/Saclay, IAS Orsay, CESR Toulouse, (France); IAAP Tuebingen, MPE Garching,(Germany); IFC Milan, ITESRE Bologna, Osservatorio Astronomico di Palermo, Italy. EPIC is funded by: PPARC, CNES, DLR and ASI. SS, GM, FD and EF acknowledge partial support by Agenzia Spaziale Italiana and Ministero della Ricerca Scientifica e Tecnologica. NG is supported by the European Union (Marie Curie Individual grant; HPMF-CT-1999-00228). KRB and JPP acknowledge the financial support of the UK Particle Physics and Astronomy Research Council.

References

Harnden, F. R. Jr., Adams, N., Damiani, F., et al., 2000, ApJL, in press

Jeffries, R. D., Thurston, M.R., Pye, J.P., 1997, MNRAS 287, 350

Micela, G. 2001, these proceedings

Micela, G., Sciortino, S., Jeffries, R. D., Thurston, M.R., Favata, F. 2000, A&A, 357, 909

Sciortino, S., Micela, G., Damiani, F., et al. 2001, A&AL, 365, in press

Strüder L., Briel, U., Dennerl, K. et al. 2001, A&AL, 365, in press

Thurston M. R. 2000, Ph. D. Thesis, University of Birmingham

Turner M. J. L., Abbey, A., Arnaud, M. et al. 2001, A&AL, 365, in press.

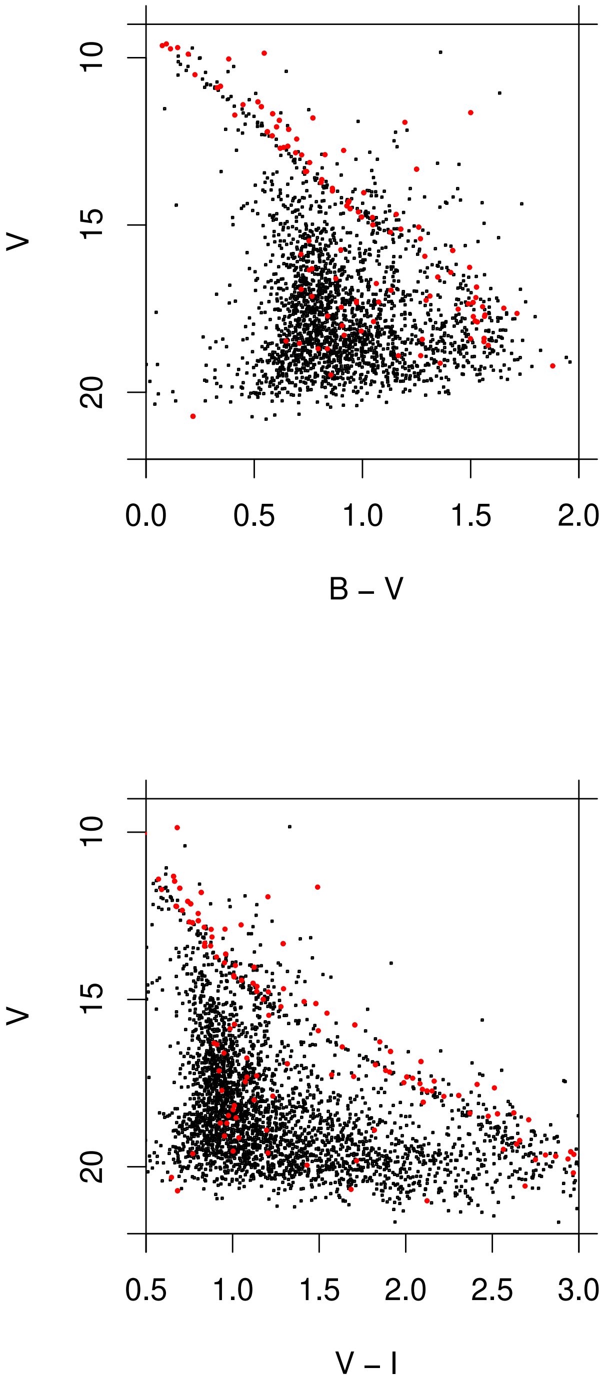

Figure 11 - CMDs for the object in the *XMM-Newton* field of view. Red symbols mark the objects identified with X-ray sources.

An X-ray flare seen with the EPIC-PN, on the early-F DK 92 star

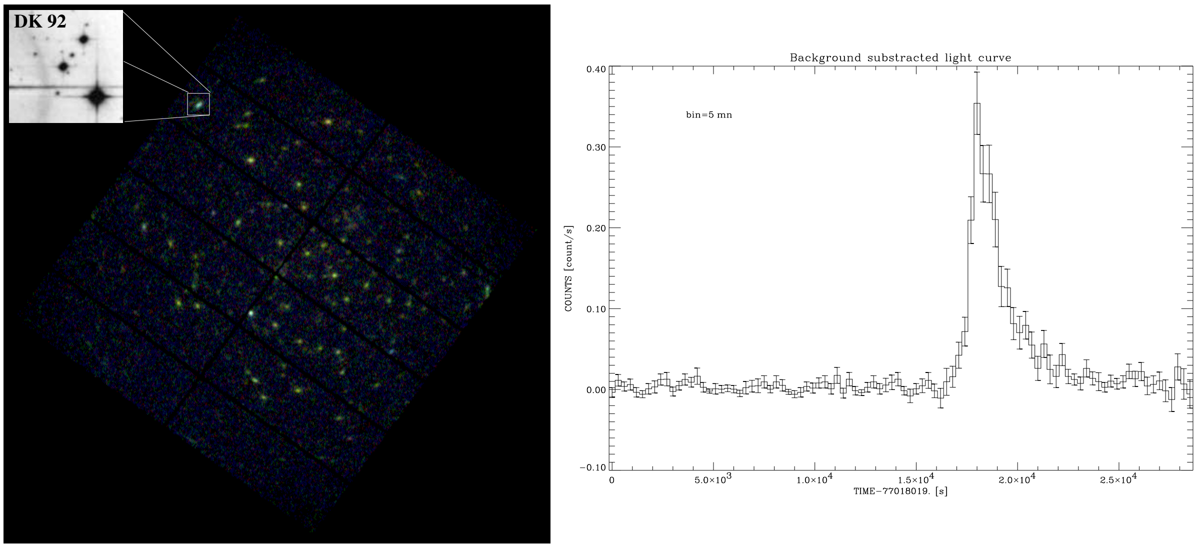

Figure 12 - Flare on the early-F DK 92 NGC 2516 member. [Right] PN image of the observation during which the flare occurs. The insert shows in optical the stars in the region around the flaring star. [Left] The light curve of the flaring star.